PostPrint

Estimation of sea state parameters by the wave buoy analogy with comparisons to third generation spectral wave models

Ulrik D. Nielsen[a,c], Jesper Dietz[b]

[a] *DTU Mechanical Engineering, Technical University of Denmark, DK-2800 Kgs. Lyngby, Denmark*
[b] *Maersk Line, DK-1098 Copenhagen, Denmark*
[c] *Centre for Autonomous Marine Operations and Systems, NTNU AMOS, NO-7491 Trondheim, Norway*

Abstract

This paper presents a study focused on sea state estimation along the route of an in-service container ship. The paper is concerned with the wave buoy analogy in which wave-induced motions of the ship are processed and analysed together with corresponding motion transfer function to give the directional wave spectrum exactly at the point of operation. In this study, a simple and inexpensive instrumentation of the vessel is considered, and wave spectrum estimation is based on measurements from one motion response unit mounted close to the forward perpendicular of the ship. The estimates by the wave buoy analogy are compared with two sets of results from third generation spectral wave models, with one set provided by a commercial supplier and with another set obtained from the Copernicus Climate Change Service Information. Motion measurements from a seven-days voyage across the Pacific Ocean are studied, and it is shown that the wave buoy analogy estimates wave conditions, in terms of sea state parameters, in good agreement with the reports by the sets of ocean wave hindcasts. Along with the comparisons, the paper discusses some of the inherent drawbacks of the wave buoy analogy, notably the fact that a ship acts as a low-pass filter.

Keywords:
Wave spectrum estimation, ship motions, wave buoy analogy, in-service data, spectral wave models, Copernicus Climate Change Service Information (ERA5)

Email address: udn@mek.dtu.dk (Ulrik D. Nielsen)

Published in Ocean Engineering, Vol. 216, pp. 107781 (2020)

1. Introduction

During ship operations, real-time and on-site estimation of sea state parameters can complement the crew's decisions to maintain high safety and fuel efficiency, since the estimate will be useful for early detection of critical sailing situations and be a crucial input to motion control systems. Similarly, attained knowledged of the sea state along the exact route of merchant ships can assist shore-based performance analysis teams towards optimising vessel and fleet performance focused on fuel consumption and environmental footprints. Moreover, estimates of wave conditions can be used for virtual hull monitoring.

One means for the estimation of sea state parameters - in real time and at the precise geographical position of a ship - considers the ship itself as a (sailing) wave buoy. This particular method is often referred to as the *wave buoy analogy*. The estimation principle of the wave buoy analogy relies on the combination of measurements of wave-induced motions of the vessel and a linear assumption, allowing the motion measurements to be modelled theoretically using transfer functions and a wave (energy density) spectrum.

1.1. Scope, highlights, and objective

The present paper studies the wave buoy analogy when it is applied together with in-service data from a larger container ship. Specifically, the estimation of sea state parameters has been made using seven days of consecutive data obtained while the ship made an east-bound trip across the Pacific Ocean with measurements from the Sea of Japan to off Graham Island (Canada). The data is obtained from a simple and inexpensive instrumentation on the vessel, where one single motion response unit, placed in a point off the centreline and close to the forward perpendicular, provides the horizontal and vertical accelerations together with the pitching motion. The corresponding motion transfer functions have been obtained from linear strip theory calculations. As a side note, it should be mentioned that the motion measurements from the specific ship have recently been used in a study about wave spectrum estimation (Nielsen and Dietz, 2020), where the sensitivity to the vessel's advance speed was investigated.

It is an inherent concern about the encountered sea state during in-service conditions that the ground truth is never known. In this study, additional estimates of sea state parameters have been obtained from spectral wave models where two sets of results are introduced; the one set is made by a commercial provider and the other set has been generated using the Copernicus Climate

Change Service Information (2020). Altogether, the highlights of the study can be referred to as (a) estimation of wave spectra, i.e. sea states, using in-service data obtained from a simple sensor instrumentation on a container vessel, and (b) a comprehensive comparison between results of the wave buoy analogy and corresponding ones produced by spectral wave models; notably the use of the freely available ERA5 data (Copernicus Climate Change Service Information, 2020) is an attractive novelty for the community working with sea state estimation, either from ship motion measurements or other means (e.g., buoys, remote sensing, wave radar systems), since the ERA5 data facilitates a comparative basis.

Despite the capabilities of the wave buoy analogy and its usefulness for (real-time and on-site) sea state estimation, as widely reported about in the literature including this paper, the current article also has as an objective to discuss some of the inherent drawbacks and problems connected to the wave buoy analogy.

1.2. Composition

The paper is organised in the following way. In the next section, Section 2, the methodology is covered and herein the fundamentals of the wave buoy analogy are outlined. The section also includes a short description of the parameters forming the background of the comparison between the results of the wave buoy analogy and the results from the spectral wave models. Section 3 presents the considered ship and its data, including the origin of the data and how it has been processed. In a model-based approach, like studied in this paper, the motion transfer functions of the vessel are of fundamental importance, and Section 4 includes a numerical examination. The results and corresponding discussions of the study are presented in Section 5, while a summary of the paper and some concluding remarks are given in Section 6.

2. Methodology

This section explains the basis of the wave buoy analogy and how Bayesian modelling, sometimes referred to as the Bayesian technique, can be used to solve the mathematical problem connected to the wave buoy analogy. The section also contains a description of the wave data made available from spectral wave models. Finally, the section introduces the sea state parameters that form the basis of the comparison between the wave buoy analogy and the results of the spectral wave models.

2.1. The wave buoy analogy - Bayesian Modelling

The assumptions and the equations governing the wave buoy analogy have been widely reported in the literature, e.g., Iseki and Ohtsu (2000); Tannuri et al. (2003); Nielsen (2006); Pascoal et al. (2007); Nielsen (2008a); Nielsen and Brodtkorb (2018). This section serves to indicate the most important aspects, while the details can be found in Nielsen (2006, 2008a).

The central assumption of the wave buoy analogy builds on linearity between waves and the wave-induced response of a vessel, and, in a frequency domain formulation, the combination with an assumption about stationarity implies the following model in which the (unknown) directional wave spectrum is $E(\omega_e, \mu)$,

$$R_{ij}\left(\omega_e\right) = \int_{-\pi}^{\pi} H_i\left(\omega_e, \mu + \beta\right) \overline{H_j\left(\omega_e, \mu + \beta\right)} E\left(\omega_e, \mu\right) d\mu + \varepsilon_{i,j} \tag{1}$$

Herein, $R_{ij}(\omega_e)$ is the response spectrum for responses i, j, where i and j correspond to any set of measured responses; say, the horizontal acceleration and the vertical acceleration, respectively, in a specific point in the ship coordinate system. The corresponding theoretical response spectrum is obtained as the product between the directional wave spectrum $E(\omega_e, \mu)$ and the multiplication of the set of transfer functions $H_i(\omega_e, \beta + \mu)$ and $\overline{H_j(\omega_e, \beta + \mu)}$ for responses i and j, with the bar denoting the complex conjugate. The mean wave-encounter angle is β and the direction of waves relative to this angle is μ, while the encounter frequency is ω_e. The error between the measured spectrum and the theoretically calculated one is $\varepsilon_{i,j}$, and it should be realised that the error in principle includes errors from sensors, transfer functions, and the model itself. Errors from sensors cannot (necessarily) be excluded, which is why fault detection techniques are relevant to consider in case of (real-time) on-board systems (Nielsen et al., 2012). Errors in the transfer functions and their influence on results can be investigated through sensitivity studies. Notably, the linear assumption, imposed through the very use of transfer functions, is a crucial factor. In this connection, reference can be made to the study by Mas-Soler and Simos (2019) addressing the nonlinearity related inaccuracies in motion RAOs when the wave buoy analogy is applied for wave spectrum estimation. The two types of errors from sensors and from the transfer functions are beyond the scope of this paper, and the paper therefore implicitly focuses only on the modelling error in the later section where data and results are presented, cf. Section 5.

It is noteworthy that Eq. (1) is usually formulated for three responses simultaneously which leads to a set of nine independent equations[1]. However, the directional wave spectrum is typically discretised into K directions and, if the 360-degrees interval is spaced by, say, 10 deg, this results in $K = 36$ unknown spectral components for any given frequency. Consequently, Eq. (1) expresses a highly underdetermined equation system that cannot be solved by minimising the error ε, as the corresponding least squares problem is ill-posed. Instead, *Bayesian modelling* can be applied to solve the equation system. The main points of Bayesian modelling are presented below but, before this, the effect of forward speed deserves special attention.

The equation system in (1) is formulated in the 'encounter domain' as the spectral densities of the wave spectrum depend on the encounter frequency ω_e, which itself is dependent on the vessel's forward speed and the wave encounter angle. As a consequence, the absolute frequency must be used instead, and it is therefore necessary to introduce the Doppler Shift. Thus, the mapping of the absolute frequency ω (of a progressive wave) to the encountered frequency ω_e is given by,

$$\omega_e = \omega - \omega^2 \frac{U}{g} \cos \mu \tag{2}$$

when the ship moves with speed U and at an angle μ relative to the progressive wave; g is the acceleration of gravity. It is noteworthy that deep-water conditions have been assumed in the present formulation. In practice, the inclusion of the Doppler Shift for problems related to general ship motion dynamics is not without complications (Bhattacharyya, 1978; Beck et al., 1989; Lindgren et al., 1999; Nielsen, 2017, 2018), but this is beyond the scope of the present paper. For wave spectrum estimation, the problem has been solved, and this is indicated in the next paragraph.

In matrix notation, Eq. (1) can be written

$$\mathbf{b} = \mathbf{A}\mathbf{f}(\mathbf{x}) + \mathbf{w} \tag{3}$$

The vector function $\mathbf{f}(\mathbf{x})$ expresses the unknown values of the wave spectrum $E(\omega, \mu)$ through a non-negativity constraint $\mathbf{f}(\mathbf{x}) = \exp(\mathbf{x})$, so that $\mathbf{x} = \ln E(\omega, \mu)$. It is noted that $\mathbf{x}$ contains $M \times K$ entries, where M is the number of discrete - absolute - wave frequencies, while K was defined previously as the number of discrete wave heading angles. $\mathbf{w}$ is a Gaussian white noise

[1]Cross spectral analysis on three discrete-time motion signals leads to 3 real-valued spectra and 6 (= 3×2) complex-valued spectra with both real and imaginary parts.

sequence vector with elements $\varepsilon_{i,j}$ which are assumed to have zero mean and variance σ^2. The vector $\mathbf{b}$ contains the elements of $R_{ij}(\omega_e)$, and the coefficient matrix $\mathbf{A}$ has elements according to the multiplication between products of the complex-valued transfer functions and the frequency derivatives $\frac{d\omega}{d\omega_e}$ obtained from the Doppler shift in Eq. (2). It should be realised that the total number of elements in $\mathbf{b}$ will be $N \times P$, where N is the number of discrete encounter frequencies and P is the number of ("fundamental") equations derived from Eq. (1); in this case $P = 3+6 = 9$ as reported previously.

In principle, the wave spectrum can be estimated from the minimisation of $g^2(\mathbf{x})$

$$g^2(\mathbf{x}) \equiv \|\mathbf{Af}\,(\mathbf{x}) - \mathbf{b}\|^2 \tag{4}$$

where $\|\cdot\|$ represents the L_2 norm. As mentioned above, Eq. (4) represents an ill-posed problem. However, by introducing Bayesian modelling (Akaike, 1980) and thereby imposing prior constraints, the wave spectrum - in terms of $\mathbf{x}$ - is basically estimated by minimising (Nielsen, 2008a)

$$h\,(\mathbf{x}) = \|\mathbf{Af}\,(\mathbf{x}) - \mathbf{b}\|^2 + \mathbf{x}^T(u^2\mathbf{H}_1 + v^2\mathbf{H}_2)\mathbf{x} \tag{5}$$

where the hyperparameters u and v control the trade-off between the good fit to the data and the prior distributions set by the matrices $\mathbf{H}_1$ and $\mathbf{H}_2$. In qualitative terms, the additional equations imposed through Eq. (5) are established by assuming the directional wave spectrum to be a smooth (piecewise continuous) function for variations with frequency and direction. Thus, the matrices, H_1 and H_2, are organised so that they ensure that the curvature of the wave spectrum is minimised (Nielsen, 2006).

In the strict application of Bayesian modelling (Akaike, 1980) it is *not* Eq. (5) which is minimised but a certain criterion - a Bayesian Information Criterion - known as ABIC. In the specific situation related to wave spectrum estimation, the criterion can be formulated (Nielsen, 2008a)

$$\begin{aligned}\text{ABIC} = P \ln h_{min}\,(\mathbf{x}) - \ln|\det(u^2\mathbf{H}_1 + v^2\mathbf{H}_2)| &+ \\ \ln|\det(\mathbf{A}^T\mathbf{A} + u^2\mathbf{H}_1 + v^2\mathbf{H}_2)| &+ C\end{aligned} \tag{6}$$

The independent variables in ABIC are the hyperparameters and the minimisation problem is thus highly nonlinear, not to mention that ABIC depends on the solution for which $h(\mathbf{x})$ is minimum. The customary practice is to solve the convolved problem brute-force; that is, for each (manually) selected combination of the hyperparameters, Eq. (5) is minimised. Obviously, this leads to a relatively high computational burden, since a range of hyperparameters must be covered for both u and v, and for each combination of the two, Eq. (5) represents an equation system with $N \times P$ equations from which $K \times M$ unknowns are solved. In the past, Sparano et al. (2008) and Nielsen and Iseki (2010) came beyond the computational burden by suggesting to use a fixed set of hyperparameters with no account for changing operational and/or environmental conditions. The selection of the fixed set of hyperparameters must be made by trial and error; and should be made in a situation when the *true* sea state is available, for instance using numerical simulations based on a specified sea state. It is noteworthy that the resulting increase in computational efficiency comes at the price of decreased accuracy from time to time. In a study, where large amount of data is analysed retrospectively for the sole purpose of comparison with other means this cost is considered acceptable.

2.2. Results from spectral wave models

Two sets of additional wave estimates, produced using third generation spectral wave models, have been collected. The one set is from a commercial supplier mainly offering their service in connection with tasks related to vessel and fleet performance analysis. The other set of result has been generated using Copernicus Climate Change Service Information (2020), noting that the dataset is a climate reanalysis, named ERA5 and based on ECMWF's Earth System model IFS. The name ERA refers to 'ECMWF ReAnalysis', with ERA5 being the fifth major global reanalysis produced by European Centre for Medium-Range Weather Forecasts (ECMWF). An overview is given by ECMWF (2020).

As a practical remark, in this paper, the term *hindcast* is often used as a reference to the estimate obtained from one of the spectral wave models.

Both sets of hindcasts comprise a number of integral wave parameters, cf. subsection 2.3, which are available every 60 minutes on a discrete spatial grid spaced 0.5 degrees in the Earth coordinates (latitude and longitude). Thus, the sets of hindcast results are (bi)linearly interpolated to the exact geographic vessel positions, cf. Section 3, for the exact time stamps in Coordinated Universal Time (UTC). The frequency and directional resolutions of the computations used by the commercial supplier are not known to the authors[2], and some additional concerns about the

[2]The ship data originates from April 2016, which was also the time when Maersk Line collected the wave data from the commercial supplier. Maersk Line never received the raw data (i.e., the wave spectra).

integral wave parameters are present, as explained in subsection 2.4.2. On the other hand, a condensed introduction to the ERA5 data is given by Hersbach et al. (2020), including ECMWF (2017), while the interested reader should consult Komen et al. (1994) for a thorough description of the equations and associated mathematical modelling related to spatio-temporal development of ocean wave spectra; as used in connection with hindcasted (and forecasted) wave spectrum estimation.

2.3. Sea state parameters

The statistics of ocean wave systems can be derived from the (directional) wave spectra characterising the particular wave systems. However, for a large data set with many samples of wave spectra, it is not practical to compare the spectra, one by one, and, besides, the actual wave spectra are available only for the wave buoy analogy and the ERA5 data but not for the commercial hindcast data, as the data supplied to Maersk Line contained integral wave parameters only. Consequently, it is decided to focus the comparative study of the different estimation methods on the basis of a set of integral wave parameters, also referred to by *sea state parameters*. On the other hand, selected samples of (directional) wave spectra by the wave buoy analogy and ERA5 are studied in the discussion of results, cf. section 5, to point out the consequence(s) of the low-pass filtering characteristics of a large ship, but a detailed comparison of the actual spectra remains as a future task.

The two sets of hindcast data contain the following sea state parameters: the significant wave height H_s, the mean energy period T_E, and the mean wave direction D_s. In case of the wave buoy analogy, which has a directional wave spectrum $E(\omega, \mu)$ as the main output, the parameters must be calculated according to their mathematical definitions,

$$H_s = 4\sqrt{m_0} \tag{7}$$

$$T_E = 2\pi \frac{m_{-1}}{m_0} \tag{8}$$

$$\widehat{D_s} = \arctan(d/c) \tag{9}$$

where

$$m_n = \int_0^\infty \omega^n F(\omega)\, d\omega \quad n = \{-1, 0\} \tag{10}$$

$$F(\omega) = \int_{-\pi}^{\pi} E(\omega, \mu)\, d\mu \tag{11}$$

$$d = \int_{-\pi}^{\pi} \int_0^\infty E(\omega, \mu) \sin(\mu) d\omega d\mu \tag{12}$$

$$c = \int_{-\pi}^{\pi} \int_0^\infty E(\omega, \mu) \cos(\mu) d\omega d\mu \tag{13}$$

It is noteworthy that Eq. (9) yields the mean wave direction $\widehat{D_s}$ *relative* to the centreline of the ship, in accordance with the definition of μ, cf. Eq. (1) in Subsection 2.1. Thus, for the wave buoy analogy, the estimate of the (absolute) mean wave direction D_s is given by

$$D_{s,WBA} = \widehat{D_s} + \Xi \tag{14}$$

where Ξ is the heading of the ship; 0 deg is North, 90 deg is East, etc.

In order to distinguish the results of the estimation methods from each other, the following notations will be used in connection with the comparisons of the sea state parameters, cf. Section 5: Results of the wave buoy analogy are referred to by 'WBA', the commercial hindcast data is denoted by 'HC', and the Copernicus data is referred to by 'ERA5'.

2.4. Notes of concern

2.4.1. The wave buoy analogy

It is important to realise that, while the integration formulas above, i.e. Eqs. (10)-(13), are given in accordance with their exact mathematical definitions, the practical computations associated with the wave buoy analogy "suffer" from the fact that the lower and upper integration limits only reflect the used cut-off frequencies as applied in the spectral calculations. This is discussed further in later sections, but the central point to note is that results of the wave buoy analogy, per se, are compromised because of two related reasons: (1) the (necessary) use of cut-off frequencies in the spectral calculations, and (2) the fact that a ship acts as a low-pass filter. In addition to these drawbacks, other issues can negatively affect results of the wave buoy analogy, as already indicated in subsection 2.1, and the later sections of the paper elaborate on this together with the comparisons of the hindcast studies (ERA5 and HC).

2.4.2. Hindcast by commercial supplier

As indicated in subsection 2.2, directional wave spectra from the commercial supplier are not available. Unfortunately, it is another concern that the total wave system is decomposed into partitions of integral parameters for swells and wind sea, respectively. For comparative reasons, it is therefore necessary to calculate equivalent wave parameters of the total wave system. In this case, the (total) significant wave height is obtained by

$$H_{s,HC} = \sqrt{H_{s,wind}^2 + H_{s,swell}^2} \tag{15}$$

The "total mean" relative direction $D_{s,HC}$ is approximated by introducing a weighted average considering the relative direction of the individual components (swell and wind sea) together with their energy content represented by the significant wave height. In this calculation, special care must be shown because directionality is circular - that is, defined on the interval [0,360[deg, where 0 deg and 360 deg correspond to the same point - and this must be accounted for in the calculation. The weighting is according to ratios of the squared values of significant wave height and, schematically, the definition of $D_{s,HC}$ is,

$$D_{s,HC} = \frac{H_{s,wind}^2}{H_{s,tot}^2} \cdot D_{s,wind} + \frac{H_{s,swell}^2}{H_{s,tot}^2} \cdot D_{s,swell} \tag{16}$$

It is possible to approximate the "total mean" energy period $T_{E,HC}$ in a similar way, and the calculation follows from

$$T_{E,HC} = \frac{H_{s,wind}^2}{H_{s,tot}^2} \cdot T_{E,wind} + \frac{H_{s,swell}^2}{H_{s,tot}^2} \cdot T_{E,swell} \tag{17}$$

Later, in the comparisons of the three sets of results (WBA, ERA5, HC) it must thus be kept in mind that the HC estimates of D_s and T_E, in the strict sense, are not (fully) consistent with the estimates by WBA and ERA5.

3. Case ship and in-service data

The case ship is a 7,200 TEU container vessel. The vessel's main particulars are listed in Table 1, and plan views of the vessel are shown in Figure 1.

Wave-induced motions of the ship have been measured with a motion sensor (XSENS, MTi-30-6A5G4), and the recordings for the study were made on an east-bound route across the Pacific

Table 1: Main particulars of the example ship.

Length between perpendiculars, L_{pp}	332 m
Breadth moulded, B_m	42.8 m
Design draught, T_d	12.2 m
Deadweight (at T_d),	76,660 tonnes
Block coefficient, C_B	0.65

Ocean, see Figure 2. The motion sensor was mounted close to the bow, off the centreline, with the exact position known by the authors. The particular sensor provides drift-free 3D orientation as well as calibrated 3D acceleration, 3D rate of turn (rate gyro) and 3D earth-magnetic field data. For the purpose of sea state estimation, the vessel's pitching motion and the horizontal and vertical accelerations have been used. The corresponding transfer functions have been calculated with an in-house linear strip theory code based on Salvesen et al. (1970), see also Section 4. In the study, the advance speed of the vessel is, as a reasonable approximation, assumed to be constant with a value of $U = 21.0$ knots at all times in the seven-days sailing period. Figure 3 shows the logged speed and, although smaller variations occur, it can be seen that it is indeed a fair assumption to use exclusively a speed of 21 knots for all 30-minutes samples forming the data stream. It is beyond the scope of the present paper, but Nielsen and Dietz (2020) discuss in detail the influence of forward speed when the wave buoy analogy is applied for wave spectrum estimation. One important finding from Nielsen and Dietz (2020) is noteworthy though; it is important to realise

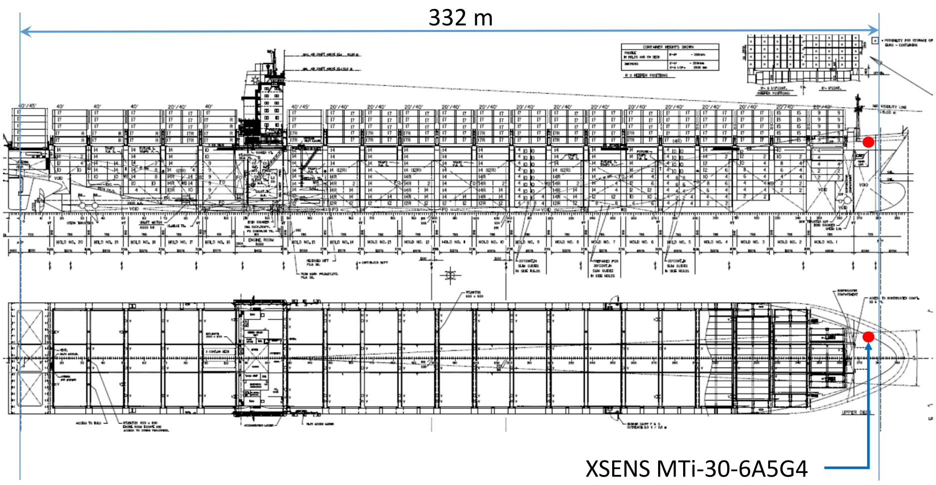

Figure 1: Plan views of the vessel with the location of the motion sensor (XSENS) indicated.

that the speed to use together with the wave buoy analogy must be the logged *speed-through-water* (STW). This point induces itself some further discussions (Antola et al., 2017; Hasselaar and den Hollander, 2017; Taudien and Bilén, 2018; Oikonomakis et al., 2019); how reliable is the logged STW from in-service vessels(?) As already indicated, the detailed discussions about forward-speed is out of the scope of this paper. Herein, reference is instead given to Nielsen and Dietz (2020) and, at the same time, noting that as part of another study (Nielsen et al., 2019b) it has been validated that the logged STW, cf. Figure 3, from the measurement period is reliable.

During the voyage, a total of 336 ($= 7 \times 48$) 30-minutes motion samples were collected. After the initial (”raw”) sampling at 100 Hz, the motion recordings were resampled to 5 Hz as the vast majority of ocean waves are observed on the interval [0-0.5] Hz; at least the waves being of importance to a +300 m container ship. Next, for each set of the 30-minutes motion samples, the cross power spectral density spectrum of the pairs of motion components was calculated using Welch’s averaged, modified periodogram method. The resulting set of nine (cross) spectra, as used for wave spectrum estimation for a single motion sample, has been limited, i.e. low-pass filtered, to the encounter-frequency interval [0.01-0.30] Hz, spaced 0.005 Hz, emphasising that no significant (wave-induced) motion occurs outside this interval. Finally, for each 30-minutes motion sample, the directional wave spectrum has been estimated, cf. Section 2.1, using a discretisation with $M = 30$ absolute wave frequencies and $K = 36$ (relative) wave directions on the intervals $\omega =$ [0.01;0.30] Hz and $\mu =$]-180;180] deg, respectively; noting that, for the relative wave direction,

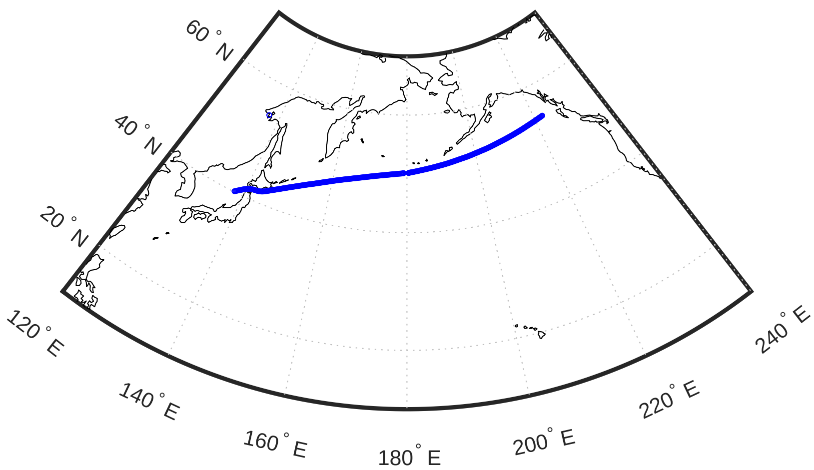

Figure 2: The analysed measurements have been recorded during an east-bound voyage across the Northern Pacific.

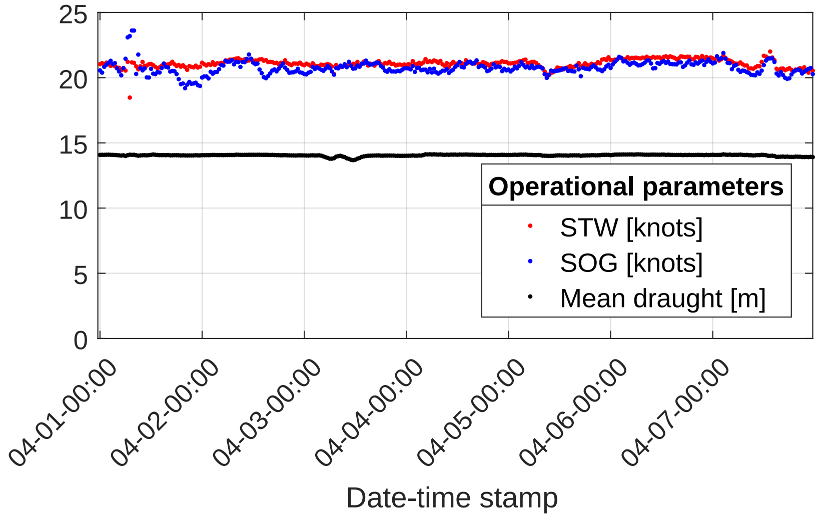

Figure 3: Measurements of advance speed during the voyage, using an acoustic Doppler current profiler for speed-through-water (STW), while GPS provides speed-over-ground (SOG). The plot includes also the logged (mean) draught amidships. The time stamps are in format 'mm-dd-hh:mm' (UTC).

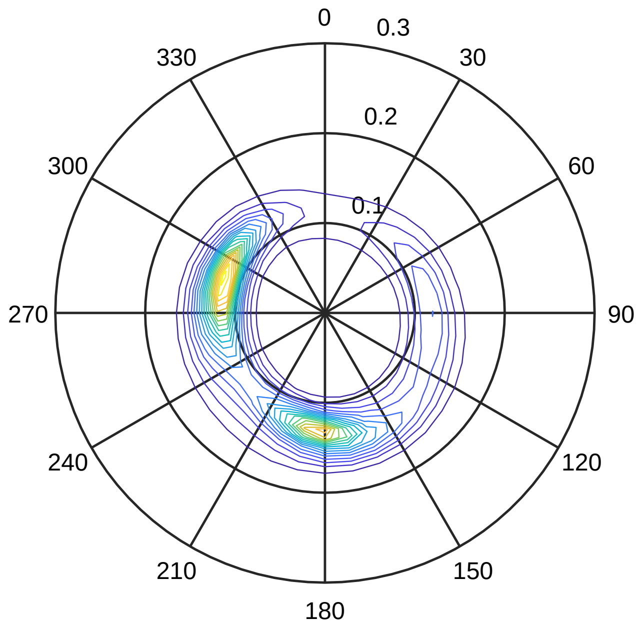

Figure 4: Directional wave spectrum estimated by the wave buoy analogy using a 30-minutes motion sample. The directional and frequency-wise energy density is indicated by colours and the directions show the directions where the energy goes to, noting that 0 deg is North, 90 deg is East, etc. In the given case, the equivalent mean wave direction is 65 deg (= where the waves come from), consistent with the sign convention of ERA5 (ECMWF, 2020).

equivalently wave encounter angle, $\mu = 180$ deg is head sea, $\mu = 0$ deg is following sea, while '+' and '-' are used to indicate if waves approach on the starboard or port side, respectively. An example of an estimated directional wave spectrum is shown in Figure 4. While detailed discussions are given later, in the given situation (sample 161) from 2016, April 4, UTC 08:00, the ship is on an 80 degrees course, which means that the wave system is coming in on the bow at the port side, i.e. bow-quartering sea. As a practical note, the solution is sensitive to the discretisation of the 'spectral domain' consisting of frequencies in the one dimension and wave heading angles in the other dimension; that is, the solution depends *conditionally* on the values of K and M and associated cut-off frequencies. Hereby is understood that if the discretisation is fine enough, the solution is stable and does not change (significantly) for a finer discretisation. For the specific ship and data, tests were made with $K = 18$ and $K = 72$ for selected cases leading to $K = 36$ as a good compromise (CPU time vs. accuracy). On the other hand, no sensitivity study has been made for M, and the cut-off frequencies, but based on the results in the next section, dealing with the motion transfer functions, the selected discretisation is considered appropriate.

4. Motion transfer functions

The motion transfer functions are of fundamental importance to the results of the wave buoy analogy. It is therefore useful to examine the behaviour of the transfer functions used for the ship in study. Figure 5 shows the modula of the three specific motions considered in the present study that uses pitch, vertical acceleration, and horizontal acceleration; repeating that the motion response unit is placed in a point close to the forward perpendicular, slightly off the centreline. As mentioned previously, the transfer functions have been computed with an in-house code, I-ship, based on the linear strip theory formulation by Salvesen et al. (1970).

In Figure 5, the modula of the transfer functions are displayed for heading angles 0-330 deg, spaced with 30 deg. In a linear theory, the assumption about rigid body motions[3] means that the local lateral motion in an arbitrary point will be a (linear) coupling of sway, roll, and yaw, and thus the lateral motion is a combination of asymmetric motion components exclusively which, in turn, implies that the *modulus* of the local lateral motion is symmetric with respect to incoming

[3]Herein, the coordinate system is a standard right-handed with surge in the forward direction of the vessel, sway to port side, and heave upwards.

waves (port side vs. starboard side). On the other hand, the local vertical motion in any point will be a coupling of heave (symmetric), roll (asymmetric), and pitch (symmetric) which means that

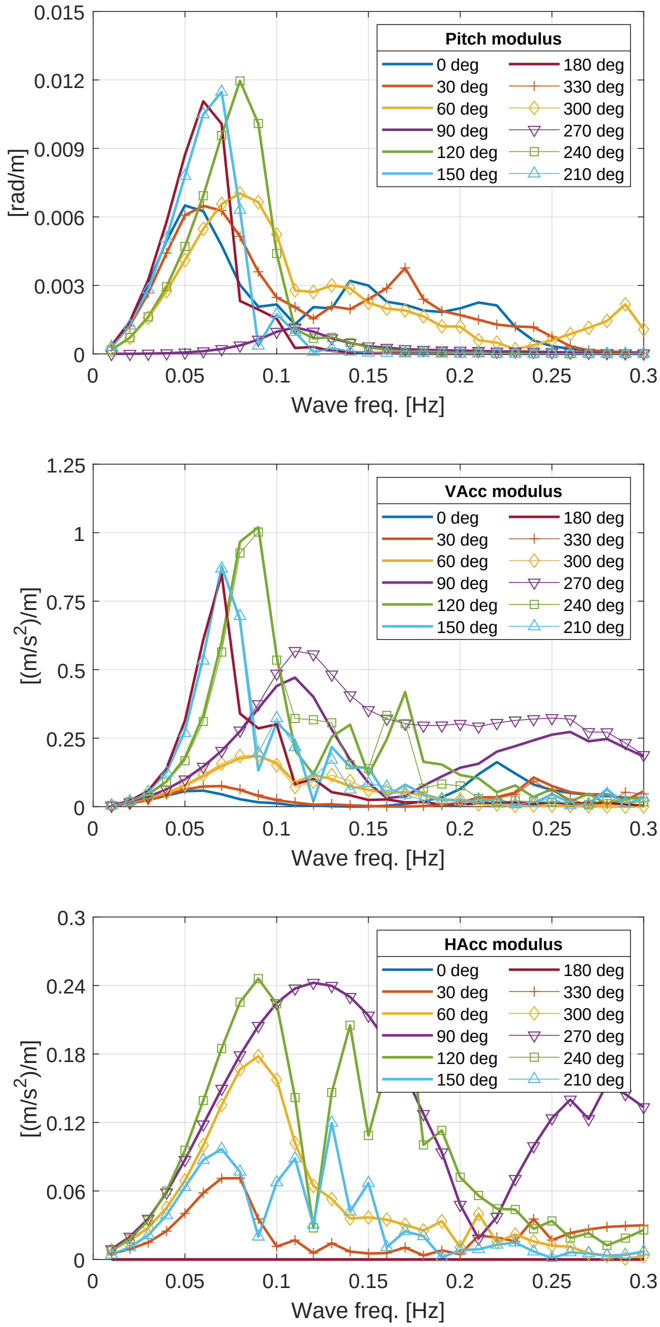

Figure 5: Modula of the three motion transfer functions (pitch, vertical acceleration, horizontal acceleration). Note, 180 deg is head sea and 0 deg is following sea.

the vertical motion is a combination of both symmetric motions and an asymmetric motion. In turn, this implies that the modulus of the local vertical motion is itself asymmetric. Summarising, the *modula* of all angular motions (roll, pitch, yaw) and all lateral local (translational) motions and derivations thereof, such as the horizontal acceleration in an arbitrary but specific point, are symmetric with respect to the direction of the incoming waves. However, vertical local motions and derivations thereof, such as the vertical acceleration, in a point off the centreline, will be asymmetric in both the argument *and* the modulus, as reflected by the middle plot in Figure 5. This makes the use of the vertical acceleration (off the centreline, close to FP) advantageous, at least in theory, because of the ability to distinguish between port and starboard incoming waves not only by the argument but also by the modulus of the transfer function; emphasising that (local) motions and other types of responses, such as wave-induced stresses (Nielsen et al., 2011; Chen et al., 2019), measured in a point exactly on the centreline can be asymmetric *only* in the argument.

Overall, it can be seen from Figure 5 that the entire set of transfer functions, considering all three responses, should be useful for 'sensing' of waves on the frequency interval [0.03-0.20] Hz, corresponding to waves with a period from about 30 s down to about 5 s. However, it is noteworthy that cases of following sea to stern-quartering sea, i.e. $\beta \approx 0 - 45$ deg (including incoming waves on either side of the vessel), do generally not impose large motions, in relative terms, which means that estimation and corresponding integral wave parameters in those cases will be of a larger uncertainty (Montazeri et al., 2015; de Souza, 2019) compared to estimations obtained when the incoming waves approach with a mean heading $\beta \approx 45 - 180$ deg from either side of the vessel.

As a final remark, due to the importance of the transfer functions in connection with the wave buoy analogy, it should be relevant to study the sensitivity to uncertainties in input parameters such as the loading condition. However, as already discussed in Section 2, this task is left as a future exercise, and the results presented in the next section are produced by taking the transfer functions to be *perfect*. In any future sensitivity studies, a number of existing works are noteworthy, e.g. Tannuri et al. (2003); Montazeri et al. (2016); Nielsen et al. (2018); Mas-Soler and Simos (2019); Nielsen and Dietz (2020).

5. Results and discussions

5.1. Comparisons of absolute values of sea state parameters

As explained in Section 2, sea state parameters, equivalently integral wave parameters, have been derived from the directional wave spectrum of the wave buoy analogy, and corresponding estimates have also been collected from two sets of hindcast data. Comparisons of all the obtained estimates are presented in Figure 6. In the plots, each point represents the result of a 30-minutes period, and from the number of chronologically-ordered sample indices (x-axis) it can be seen that data covers a seven-days consecutive period corresponding to the sailing time and traveled distance, cf. Figures 2 and 3. Generally, reasonable agreements are found between the different estimation methods (WBA vs. HC vs. ERA5), which is a finding that applies to all three sea state parameters; that is, significant wave height H_s (upper plot), mean energy period T_E (middle plot), and mean wave direction D_s (lower plot).

It is noteworthy that the commercial hindcast data (HC) has no parameters in a 5-hours period around samples 182-192. While the exact reason is unknown, since the authors do not hold the raw data themselves, a likely explanation could be related to the crossing of the date line. Similar observations can be found in the beginning of the date stream (samples 20 to 30), where there also appears to be a few values missing for the HC data provided by the commercial supplier. In this case, the explanation is likely because land points are not properly treated; noting that the vessel is close to land (the island of Hokkaido) during the particular time stamps.[4] While values of the wave buoy analogy are not missing at any instants, there are, however, observations of sudden jumps in the data. This is primarily observed for the mean wave direction, and is likely a result of modelling errors. In fact, previous reports of the wave buoy analogy have reported about problems to estimate the (mean) wave direction, and it has often been found that, among the sea state parameters, the largest inaccuracies are connected to the estimation of the *directional* distribution of energy density (cf. Figure 4), equivalently the wave direction. The reason for this has been studied and discussed by Iseki and Nielsen (2015); Hong et al. (2018, 2019), and it is considered that short-term variability, due to aleatory uncertainty, in the actual wave elevation sequences is responsible for the problems associated with (incorrect) estimation of the wave direction from time to time. The explanation is that short-term variability severely affects the phase difference between

[4]Thanks to an anonymous reviewer to point out the problems with the date line and land points.

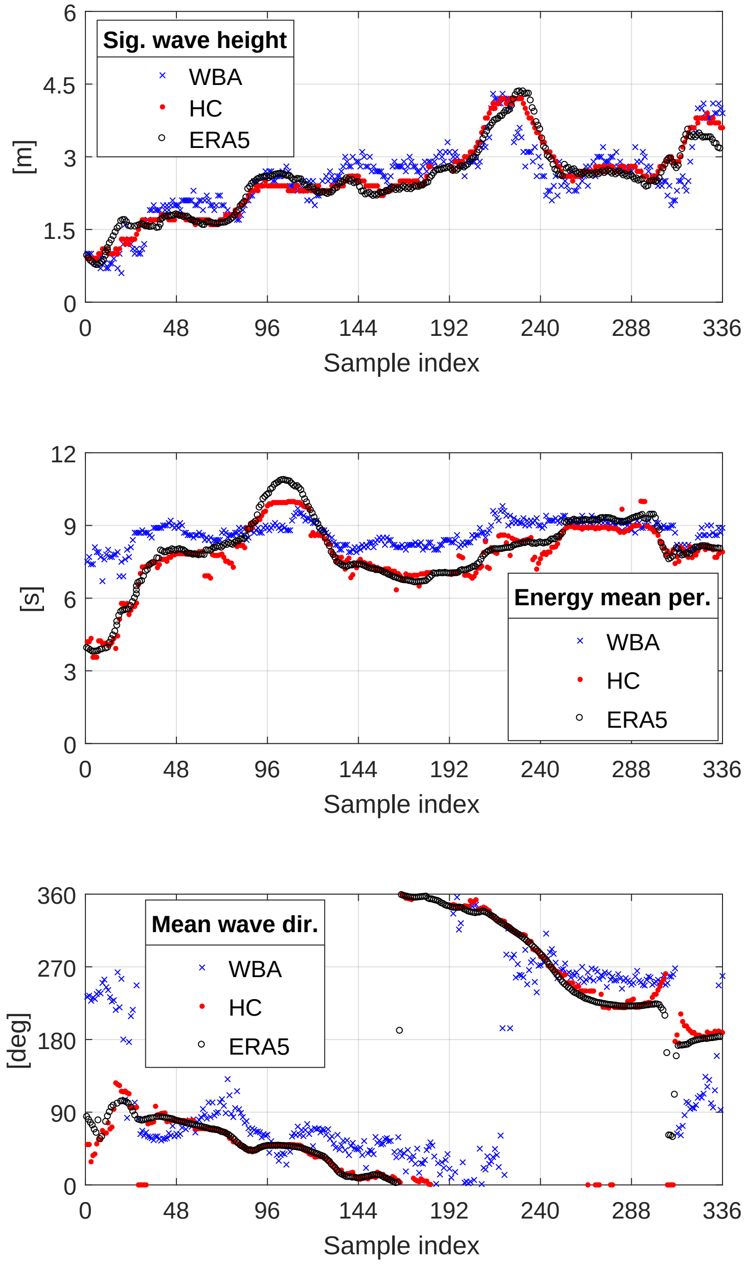

Figure 6: Estimated sea state parameters as obtained from the wave buoy analogy (WBA), the commercial hindcast (HC), and the Copernicus Climate Change Service (ERA5). The upper plot shows the result for significant wave height (H_s), the middle shows mean energy period (T_E), and the lower plot shows the mean wave direction D_s (where the waves come from).

the wave-induced motion components, such as heave and roll, and, thus, short-term variability is harmful for the estimation of the directional distribution of energy density. This is so because it is the phase difference between the motion components that gives the cross spectra used in the governing equation, cf. Eq. (1), and it is in turn the cross spectra that facilitate (accurate) estimation of wave direction.

One particular observation deserves additional comments: When the data around samples 216-240 is studied, there appears to be something looking almost like a "time shift" in the estimates of H_s; comparing WBA with both sets of hindcasts. However, it is believed that the apparent time shift is simply a coincidence, since it has not been possible to find any explanation related to a mismatch in time/position. In addition, the "time shift" is not observable in the estimates of T_E and D_s, them being neither worse nor better. On the other hand, somewhat remarkable, the behaviour ("time shift") occurs as the wave system gradually changes from propagating from a northerly (360 deg) to propagating from a westerly (270 deg) direction, which means that, relatively, the vessel goes from being in beam sea to being in following sea, noting that the ship sails East (cf. the route map in Figure 2). The change in wave direction leads to changes in the motion dynamics of the vessel, and the effect(s) of 'wave filtering' by the wave buoy analogy is therefore the likely cause for the particular observation resembling a "time shift" in H_s.

The agreement between the estimation methods is visualised in Figure 7 that shows correlation-types of plots and, thus, can be used to directly evaluate the methods against each other. Not surprisingly, the best agreement is observed between the two sets of hindcast data; noting that the hindcast results are based on the same kind of modelling using the full *energy balance* equation (Komen et al., 1994). Generally, the deviations between the two sets of hindcasts (ERA5 vs HC) are small, notwithstanding it is believed that the more significant deviations are due to the calculation of *equivalent* total integral wave parameters for the data by the commercial supplier, cf. subsection 2.4.2. The results of the wave buoy analogy agree reasonably well with the hindcast data when the significant wave height is considered, and there appears to be no particular trend as the scatter is random for the range of wave heights from about 0.5 m to about 4.5 m. Having a focus on the wave period, i.e. T_E, it is evident that the results from the wave buoy analogy and from the sets of hindcast are less consistent. Notably, it can be seen that the wave buoy analogy tends to produce (too) high periods, except from a few cases around samples 85-120 (see later). This observation is (again) a consequence of the fact that any ship acts as a low-pass wave filter, since the resulting wave-induced motions of a ship depend on its size relative to the wave length. In practice, this

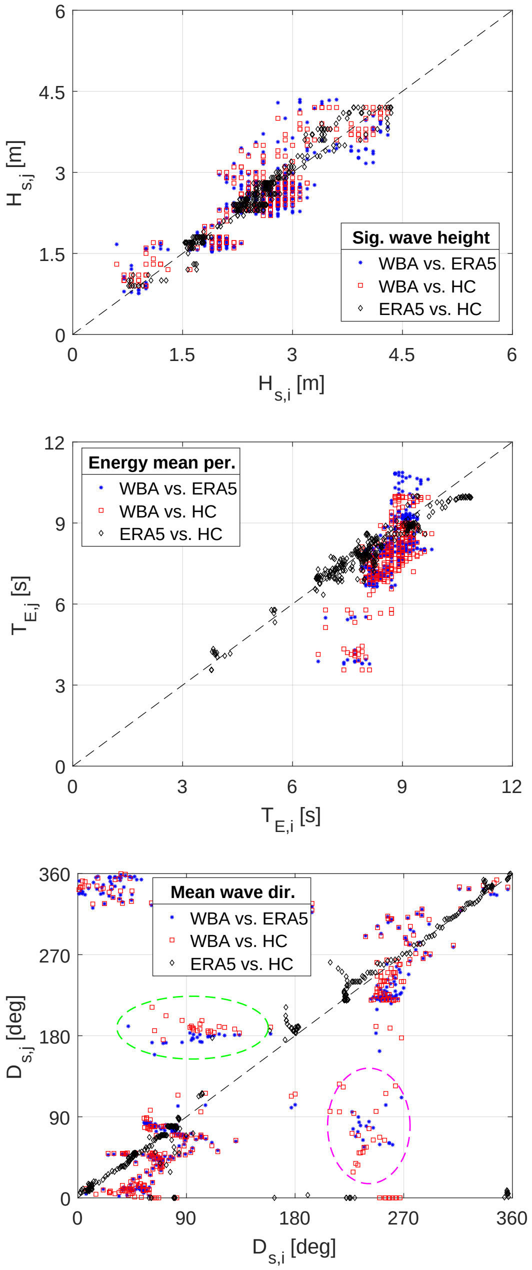

Figure 7: Direct comparisons between the estimation methods for significant wave height (top), mean energy period (middle), and mean wave direction (bottom). The pairwise comparisons are indicated by the legends, where the former estimation method, i, for a compared pair, 'i vs. j', is given on the x-axis, while estimation method j is given on the y-axis.

means that, when the wave buoy analogy is applied with larger ships, there is a tendency that the higher-frequency wave components of a wave spectrum are "filtered away", and the result is that the tail of the wave spectrum is cut short.

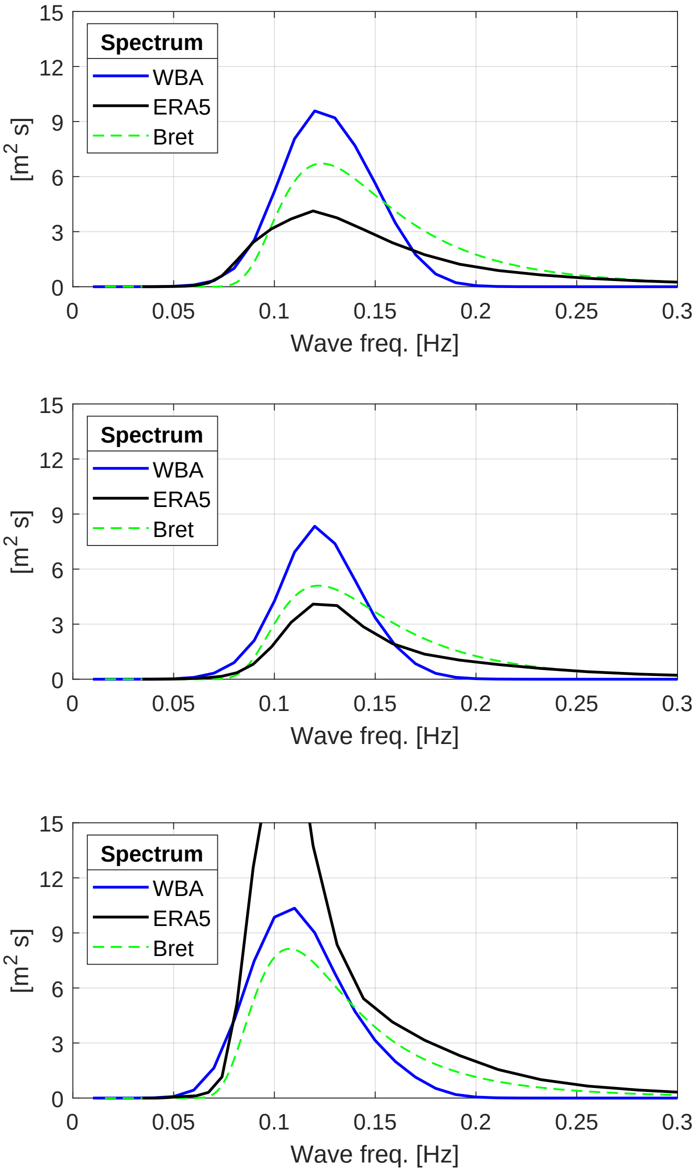

Figure 8: Examples of 1-D wave spectra to illustrate the (low-pass) filtering aspects of the wave buoy analogy compared to ERA5. The spectra correspond to samples 137, 161, and 233. The plots include comparisons to a standard spectral shape of a Bretschneider spectrum (Bret) with identical wave parameters H_s and T_p as produced by the WBA.

This particular finding can easily be observed from plots of (1-D) wave spectra, and Figure 8 illustrates a few (arbitrarily) selected cases from the considered data of this study. The plots contain comparisons between WBA and ERA5[5] shown together with a Bretschneider spectrum (Beck et al., 1989) produced with identical wave parameters as estimated by the WBA. From the plots in Figure 8 it is noted that the specific vessel does not really respond to waves with a frequency higher than about 0.20 Hz (for any wave heading) resulting in a tail on the WBA spectra which is cut short at this frequency. This "cut-off" frequency is confirmed by inspection of the motion transfer functions referring to Figure 5. In the shown cases in Figure 8, the ERA5 spectra are seen to have tails that match well the Bretschneider shape. It is thus an inherent problem of the wave buoy analogy that it produces wave spectrum estimates where the characteristic wave frequency (respectively wave period), tends to be on the lower side (respectively higher side). The particular disadvantage will be the most pronounced in developing wave systems where the waves are relatively short compared to vessel size. In this context it is important to mention that techniques against the low-pass filtering characteristics of ships in connection with the wave buoy analogy have been studied (Nielsen, 2008b; de Souza et al., 2018). The idea is to use other types of responses than merely global wave-induced motions but, as this requires additional sensors not installed on the specific ship of this study, no further attention is given to the topic. It is noteworthy that all the shown WBA 1D wave spectra in Figure 8 have a single and distinct peak, although the Bayesian technique, as indicated in Section 2, allows several peaks in the solution, frequency-wise as well as directional-wise, corresponding to a mixed sea consisting of both swell(s) and wind waves from multiple directions. However, in the particular cases in Figure 8, the Bayesian technique - apparently - 'prescribes' a (unimodal) sea consisting of wind waves exclusively. On the other hand, the middle 1D spectrum (sample 161) in Figure 8 is the integrated version of the directional wave spectrum shown in Figure 4, where it can be seen that two (distinct) spectral peaks exist at different directions but at the same frequency, indicating that, indeed, it is a mixed sea with waves from two different directions. In fact, the two other cases of 1D spectra in Figure 8 also represent sea states with waves coming from more than just one direction. Based on the preceding discussion about filtering (and the possibility to estimate multi-modal wave spectra with the Bayesian technique), it

[5]It should be acknowledged that the authors were kindly supplemented the (directional) ERA5 spectra by an anonymous reviewer.

would obviously be interesting to study the actual wave spectra obtained from the hindcast studies, and subsection 5.3 contains preliminary results in this direction. To finish the discussion about T_E - and the tendency to overestimate - it should be noted that there is a sequence of samples ($\sim 85 - 120$) where T_E is consistently underestimated, thus contradicting the above discussion. It has not been possible to properly explain this observation, especially since there appears to be noting peculiar in the estimates of the two other parameters (H_s and D_s). On the other hand, the "inconsistency" coincides exactly with a period, i.e. samples 85-120, where the mean wave direction, as reported by ERA5 and the HC result, initially drops a little bit and then remains to be fairly constant around 45 deg, corresponding to waves coming from northeast. Having the ship's course in mind (sailing eastwards), the underestimation of T_E is therefore happening in cases of bow-quartering waves on port side. The data does, unfortunately, not include cases corresponding to bow-quartering waves on starboard side, so it is left as a future work, by analysing data from other voyages, to study if there is any relation between the underestimation of T_E and the vessel being in bow-quartering waves.

Returning to Figure 7, the plot at the bottom shows the agreement between the wave buoy analogy and the hindcast data when the mean wave direction is considered. Despite the apparent scatter, the agreement is fair for most of the data, as directional ambiguity implies that wave directions 0 deg and 360 deg are identical; both values represent waves propagating from North. On the other hand, a mismatch is observed for the cluster of points located within the green-dashed ellipse. It is seen that, for this cluster, the wave buoy analogy estimates wave directions primarily in the range 90-135 deg, i.e. coming from east-southeast, while the hindcast data reports wave directions in a quite narrow range around 180 deg. It is noteworthy that the particular cluster of points corresponds roughly to samples 300-336, and the disagreement is seen easily also in Figure 6 in the bottom plot. Similarly, in Figure 7, there is a cluster of points, located within the magenta-dashed ellipse, where the agreement between the wave buoy analogy and the hindcast data is poor. In this case, the wave buoy analogy makes estimates of (mean) wave directions mainly in the range 225-270 deg, i.e. waves coming from west-southwest, while the hindcast data reports wave directions around 45-150 deg; that is, a 180 deg mismatch in some cases. In fact, for the magenta-dashed ellipse and with the ship's route in mind, cf. Figure 2, the estimates by the wave buoy analogy represent following to stern-quartering waves, whereas the reports from the hindcast data

Table 2: Mean value and standard deviation of the absolute errors, cf. Eq. (18), between the sea state parameters estimated by the different estimation methods, when compared pairwise.

	ΔH_s [m]		ΔT_E [s]		ΔD_s [deg]	
Error	Mean	Std	Mean	Std	Mean	Std
WBA vs. HC	0.00	0.36	0.84	0.98	3.6	59
WBA vs. ERA5	0.06	0.43	0.66	1.05	15	52
HC vs. ERA5	-0.05	0.17	0.14	0.36	-3.4	27

correspond to head to bow-quartering waves. The disagreement of the magenta-dashed cluster of points in Figure 7 is observed as well from Figure 6 where the particular cluster of points roughly corresponds to samples 1-30. The discussed disagreements in the wave heading has been indicated (already) in connection with the examination of the motion transfer functions, cf. Section 4, where it was reported that the vessel, according to the motion transfer functions, sees relatively little response around wave headings from following to stern-quartering waves.

5.2. Error statistics of comparisons

The comparative study of the estimation methods has been summarised in Table 2, where the statistics of the errors between corresponding sea state parameters are shown. In the table, the mean value and the standard deviation of the absolute errors between different estimation methods i and j are presented; noting that errors are calculated between the pairs of methods 'WBA vs. HC', 'WBA vs. ERA5', and 'HC vs. ERA5'. Thus, the single error ϵ between a pair of estimates, i vs. j, for a given parameter α, for time sample k is defined by

$$\epsilon_{\alpha,k}^{\{i\ vs.\ j\}} = \alpha_k^{\{i\}} - \alpha_k^{\{j\}} \ , \quad \alpha \equiv \{H_s, T_E, D_s\},\ k = 1 : N_t \tag{18}$$

The mean values and standard deviations of the error are obtained by summing up over all time samples; $N_t = 336$ is the total number of 30-minutes time samples in the data (seven days). It is decided to focus on absolute errors rather than normalised ones. Moreover, it is noteworthy that the ambiguity in wave direction is accounted for by subtracting or adding 360 degrees if the error is larger or smaller, respectively, than 180 degrees. The basis of the 'summarising numbers' in Table 2 is presented in Figure 9 that shows the complete sets of *normalised* errors relative to the ERA5 data; additional comments are given later.

Table 2 (and Figure 9) confirm the previous findings reported together with Figures 6 and 7. Specifically, it is observed that, on average, the wave buoy analogy yields estimates of significant wave height in good agreement with the two sets of hindcasts (HC and ERA5) with mean values on the errors at 0.0012 m and 0.06 m. However, the two sets of hindcast data are generally more consistent in their estimates with a smaller standard deviation on the error being 0.17 m. It is also evident from the numbers in Table 2 that the two sets of hindcast results (HC vs. ERA5) are in better agreement when estimates of mean energy periods and mean wave directions are considered as the mean values of the errors are 0.14 s and -3.4 deg, respectively, on T_E and D_s. When results from the wave buoy analogy are compared to the hindcast results on these parameters, it is interesting to observe that the mean values of the errors, i.e., WBA vs. HC, and WBA vs. ERA5, are at a reasonable level with values 0.84 s and 0.66 s on T_E and 3.6 deg and 15 deg on

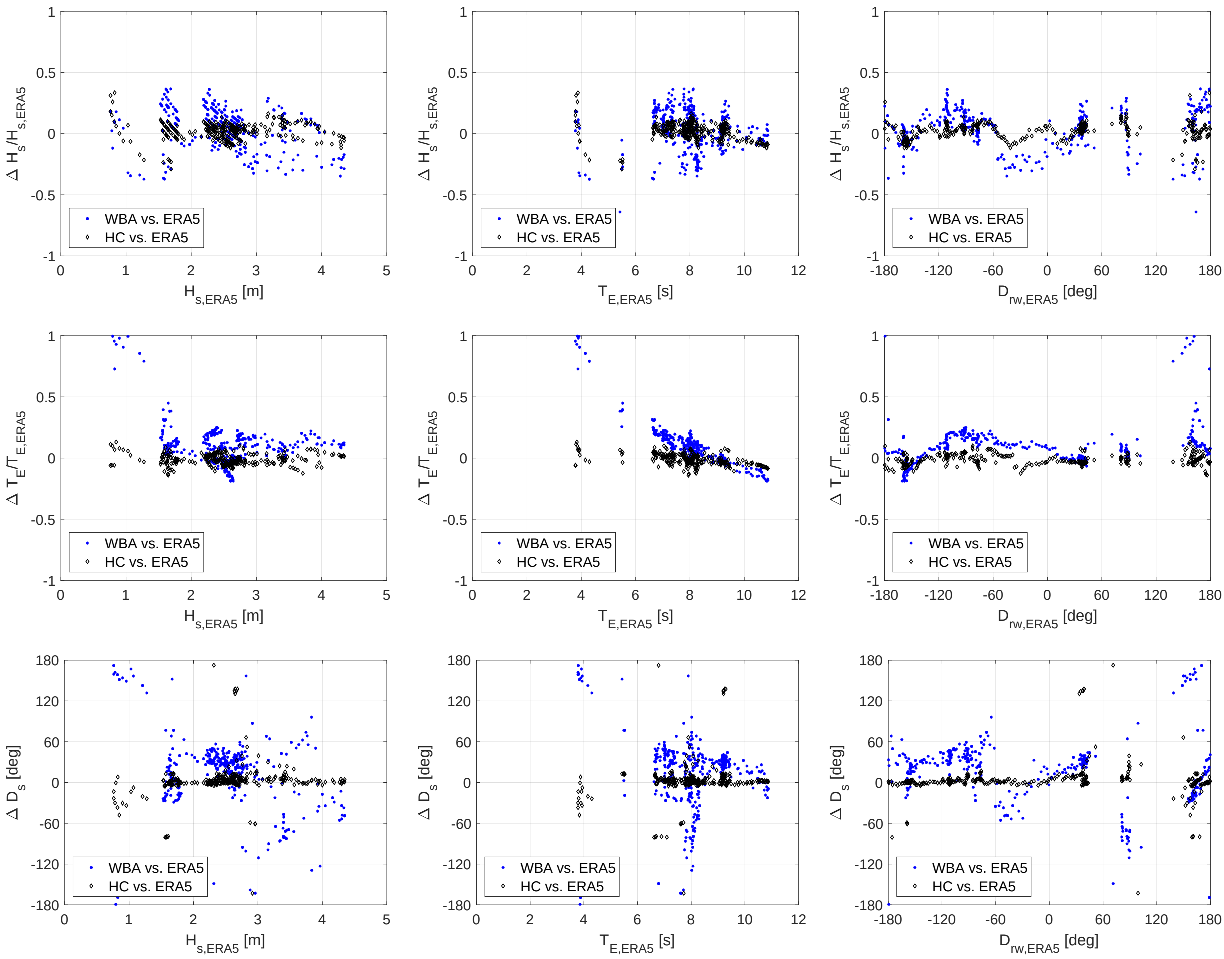

Figure 9: Illustration of the relative error between results of the wave buoy analogy and the ERA5 data (WBA vs. ERA5), and between results of the two sets of hindcasts (HC vs. ERA5). The relative wave direction $D_{rw,ERA5}$ is computed similar to Eq. (14).

D_s. On the other hand, the results are less consistent resulting in larger standard deviations. The reason for this observation is primarily related to the two clusters of data marked by the green and magenta-dashed ovals in connection with the bottom plot of Figure 7.

As mentioned previously, Figure 9 presents plots of the single errors used for the production of Table 2. Specifically, plots are shown for the normalised errors of H_s (top row) and T_E (middle row), using the ERA5 data as basis, and for the absolute errors of D_s (bottom row); in all cases as function of the ERA5. The left-side column of plots shows the errors as function of the significant wave height, while the middle column of plots shows the errors as function of the mean energy period. The right-side column of plots shows the errors as function of the relative wave direction, where 180 deg represents head waves and 0 deg is following waves, with + and - to distinguish between waves approaching on the starboard side and port side, respectively. It can be seen that the only notable trend, as discussed earlier, is observed for errors in the mean energy period, where it is evident that the wave buoy analogy, due to filtering characteristics of the motion transfer functions, cf. Section 4, produces results higher than the ERA5 data, when the wave period is low. Moreover, it can be observed that cases, where WBA overestimates the most the T_E parameter, correspond not only to low wave periods, but also to low significant wave heights (left middle plot). Somewhat peculiar it can be seen that the wave buoy analogy and also the commercial hindcast yield a mean wave energy period which is lower than the estimate from the ERA5 data for the higher wave periods; or, in other words, the ERA5 mean energy period might be slightly on the larger side, when the wave period is high(er).

5.3. Additional discussions about the effect of wave filtering

It is evident that wave filtering affects the estimates by the wave buoy analogy. The effect is an inherent concern that results because of the motion characteristic of the given vessel, cf. section 4. As such, different vessels of different dimension will not imply the same "deterioration", and estimates are typically better/worse depending on the relative size of the vessel compared to wave length (Nielsen et al., 2019a). In general, it is difficult to evaluate exactly to which degree the estimates by the wave buoy analogy are (negatively) affected by filtering. However, by use of the ERA5 data it is possible to get an indication.

In the preceding, the integral parameters associated with the ERA5 spectra were obtained *per download*, directly from the (CDS) data store, noting that the parameters are pre-computed (*in* the CDS) by integrating over the full frequency range, i.e. up to 0.55 Hz, for the given the spectra (ECMWF, 2017). As an alternative, the ERA5 parameters can be obtained by limiting the integration up to 0.2 Hz; corresponding to imposing a cut-off frequency approximately equivalent to the "filtering-induced" cut-off frequency used with the WBA. The results of these computations are shown in Figure 10 with curves for the significant wave height and the mean energy period, where it is observed that the cut-off frequency, by nature, implies an increase in H_s and a decrease in T_E. It is observed that the impact seems mostly on the mean wave period, while the impact on significant wave height is less pronounced. The consequence of this finding, in relation to the wave buoy analogy, is illustrated in Figure 11. In the plots, results are included for both sets of the ERA5 parameters; i.e. the normal integration over the full frequency range and the integration limited to an upper cut-off frequency of 0.2 Hz. By visual inspection, it is clear that the agreement in H_s reduces slightly ("normal" vs. "limited integration"), while the agreement in T_E improves. The agreement can be quantified by calculating normalised root mean squared (RMS) errors, making the error relative to the true ERA5 parameter obtained from integration over the full frequency range. The results are $\text{RMS}_{Hs} = 0.14$ (normal) and $\text{RMS}^*_{Hs} = 0.18$ (limited) for significant wave height, and $\text{RMS}_{Te} = 0.15$ (normal) and $\text{RMS}^*_{Te} = 0.09$ (limited) for mean energy period. Thus, Figure 11 supports the previous findings in the sense that the main concern with the wave buoy analogy is the, at times, inconsistent *distribution* of energy densities.

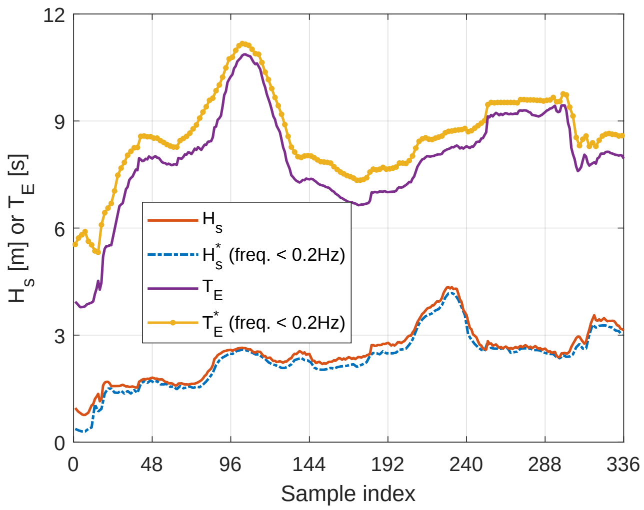

Figure 10: The effect on ERA5 H_s and T_E by imposing a cut-off frequency at 0.2 Hz.

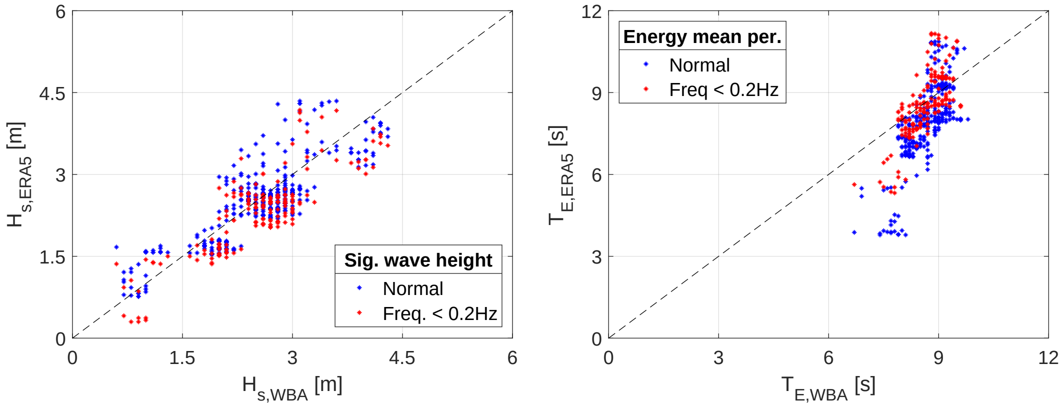

Figure 11: Comparisons between sea state parameters by the wave buoy analogy (WBA) and by ERA5 with two different sets of parameters for ERA5.

As mentioned in subsection 2.3, it will be left as a future task to make the detailed comparison between the directional wave spectra by the wave buoy analogy and the corresponding ones from ERA5. However, Figure 12 contains a few glimpses of arbitrarily selected examples; albeit the selected ones correspond to the three cases shown in Figure 8 and one additional case from the end of the data stream (sample 313). For completeness, the 1D spectra are included, although subfigures (a)-(c) are similar to the plots in Figure 8. Suffice it here to say that the (comparisons of the) directional spectra reveal an agreement of the detailed energy density distribution, somewhat in line with what can be expected for estimates *not* from the exact same physical position (nor time stamp); see further below. It is noted that the modal frequency of the directional spectra (ERA5 vs. WBA) to some degree matches; with the exception of sample 313 (subfigure d) which is an outlier in this respect. In further works, it should be attempted to study what the causes are for the observed inconsistencies. One explanation could be due to nonlinear effects (wave-ship interactions), which are not considered because of the use of (linear) transfer functions in the wave buoy analogy. However, it is also important to realise that it has not been attempted to interpolate the ERA5 spectra to the actual coordinates of the ship[6]. This means that the ERA5 wave spectra apply to the fixed grid points used in the ECMWF spectral wave model, and, therefore, the sole difference in physical location might be responsible for the (smaller) inconsistencies in the directional energy density distribution. The implication of (spatial) distance between estimates of directional wave

[6]Such an interpolation algorithm would require consideration of effects from wave dispersion, current, wind, etc.

spectra is also observed by, for instance, Stredulinsky (2010), where it can be seen that, albeit the mean wave direction agrees fairly well, notable differences may exist in the peak wave direction,

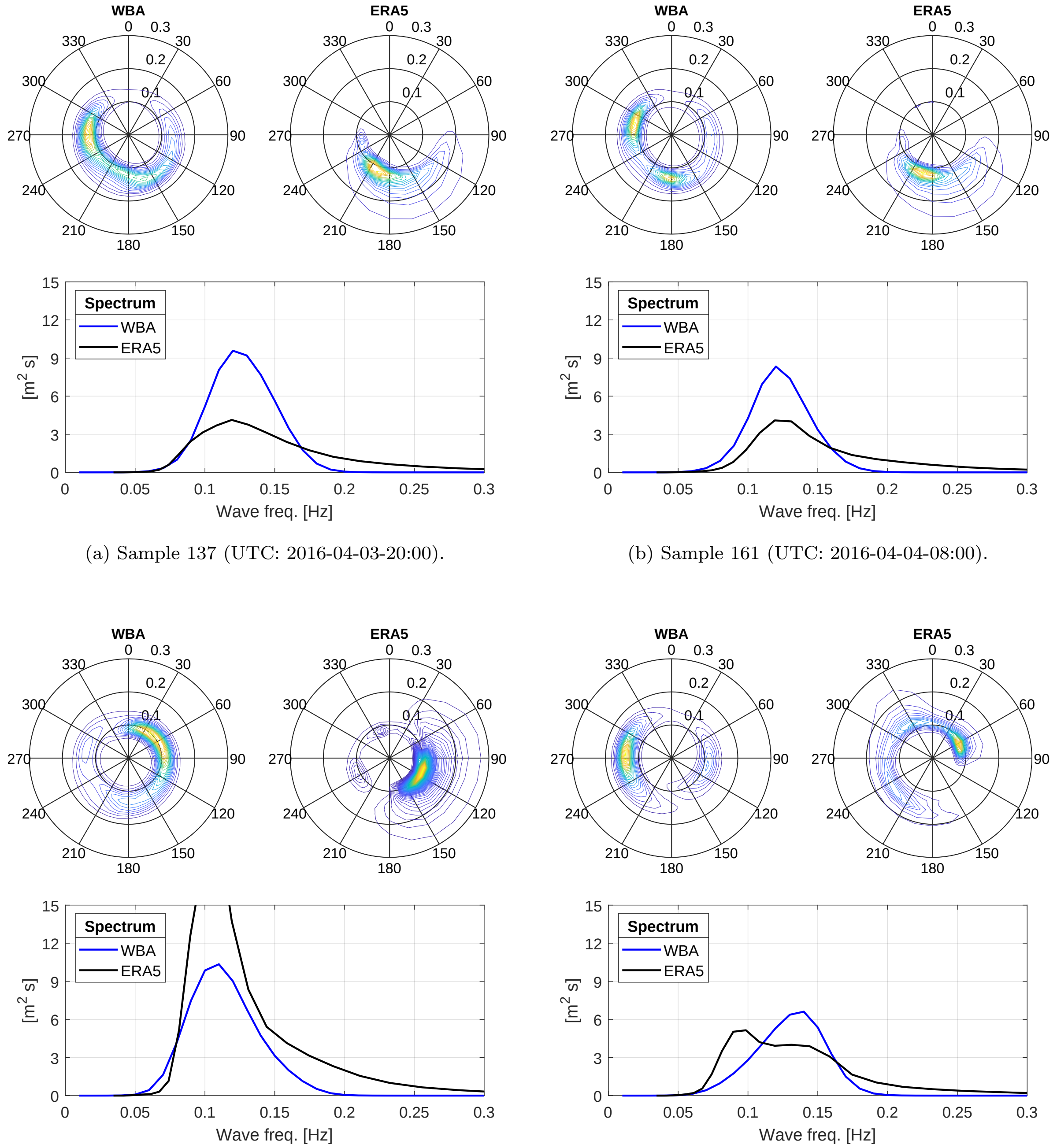

(a) Sample 137 (UTC: 2016-04-03-20:00).

(b) Sample 161 (UTC: 2016-04-04-08:00).

(c) Sample 233 (UTC: 2016-04-05-20:00).

(d) Sample 313 (UTC: 2016-04-07-12:00).

Figure 12: Examples of wave spectra with comparisons between the wave buoy analogy (WBA) and ERA5, both 2D and 1D spectra. Note, in the plots of 2D spectra, the directions are giving the directions where the energy is going.

when estimates by two wave buoys are compared; noting that the buoys are spaced only a few kilometers (2-40 km) apart. In some of the presented cases (Stredulinsky, 2010), the two buoys disagree up to 90 deg in the location of the peak.

5.4. Remarks about validation of sea state estimates

As indicated several times already, the comparison of ocean wave conditions is difficult, since the ground truth is not available; although measurements from real wave buoys are often considered close to. Nonetheless, in the preceding, the ERA5 was used as basis and, by all means, it seems reasonable to assume that results of (third generation) spectral wave models are generally closer to the ground truth than estimates by the wave buoy analogy. In this line, it seems relevant to mention that different types of validation of the ERA5 data have been made by Hersbach et al. (2020) to justify the use of ERA5 as basis. As a related comment, use of satellite data, i.e. space-borne SAR, could also be interesting to look at for comparisons in future studies. In fact, satellite data was used in the study by Nielsen (2006) that revealed a fair agreement. It is important, however, to keep in mind that, like the wave buoy analogy, space-borne SAR cannot retrieve properly integral wave parameters corresponding to the complete frequency range, since SAR observes only part of the low frequency wave spectrum.

6. Conclusions and final words

In this paper, the wave buoy analogy has been applied to estimate the sea states encountered by a container ship during a seven-days crossing of the Pacific Ocean. The basis for the estimation was measurements from a motion response unit placed at a point off the centreline and close to the forward perpendicular together with motion transfer functions calculated by strip theory. Thus, instrumentation and necessary software are simple and inexpensive compared to the alternative technology for real-time and on-site wave estimation from (in-service) ships; namely wave radar systems (Nieto-Borge et al., 1999). The main conclusions of the study are listed below, and some further works are suggested in addition to the future studies already discussed at various occasions in the paper.

In the study, the sea state estimates - in terms of integral wave parameters - by the wave buoy analogy were compared to two corresponding sets of estimates obtained from third generation spectral wave models. The results of the spectral wave models were referred to by hindcasts, and in the study the hindcasts collected from a commercial supplier and from the Copernicus Climate Change Service Information were considered. Generally, good agreement exists among the estimates, however, with the best correlation between the two sets of hindcast data; noting that this is expected as the two sets are based on the same kind of modelling using the full energy balance equation. From the quantified comparison between the wave buoy analogy and the two sets of hindcast data, it was clear that the wave buoy analogy often produces directional wave spectrum estimates having the same total *amount* of energy, given in terms of the significant wave height (H_s), and with no particular trend. On the other hand, the estimation of the *distribution* of energy (density), reflected by the mean energy period (T_E) and the mean wave direction (D_s), is made with a reduced agreement, when results by the wave buoy analogy are compared to results produced by hindcasts. The reason for this observation is mainly because of the filtering effect of a ship; leading to a cut-off of the tail of the wave spectrum. Consequently, future studies on the wave buoy analogy should try to address this problem. In this relation, existing work (Nielsen, 2007; de Souza et al., 2018; Nielsen et al., 2019a) focused on the use of different sensors and using multiple size-varying ships could be further studied. Alternatively, in the same context, it could be a possible solution to make a (mathematical) fit of the tail of the wave spectrum; emphasising that the fitting should be made just for the (higher) frequencies where there generally is no significant motion response in accordance with the transfer functions. This approach would be somewhat consistent and similar to what is done in the spectral wave models that assume a high-frequency tail above the last resolved frequency (0.55 Hz for ERA5).

In contrast to new developments directly focused on the wave buoy analogy, it would be of interest to study how much variation the hindcast results, such as the ERA5 data, shows between the single, discretised (geographical) coordinates in which the data is referred to. Herein, it is understood that hindcast data, strictly speaking, is valid only in the points of the geographical grid, in this study spaced by 0.5 degrees (longitudes and latitudes), while the hindcast estimate at an arbitrary point, as an approximation, has been obtained by bilinear interpolation. This approximation should be tested further by examining the hindcast estimates in several neighboring grid points, and, in addition, by studying if the agreement between the wave buoy analogy and the hindcast result(s) depends on the distance to the grid points. In fact, preliminary studies in this direction have been initiated (Nielsen and Holt, 2020). As a somewhat related remark, it is noted that when a ship advances with a speed of more than 20 knots, the distance covered in, say, 30 minutes is about 20 km. Obviously, the assumption about stationary conditions can be questioned; despite a constant ship speed and heading, the seaway itself can change. It should therefore be worthwhile to focus attention towards (higher order) spectral analysis methods applicable during nonstationary conditions (Iseki and Terada, 2003; Iseki, 2010, 2012; Takami et al., 2020).

Acknowledgment

The authors would like to acknowledge that vessel motion data was collected together with Propeller Control ApS through the Blue Innoship Project 2, which was supported by the Danish Innovations Fund, the industrial partners and the Danish Maritime Fund. Thanks are directed to Jos Koning (MARIN) for answers and clarifications about the sensor installations and data collection. Furthermore, the fruitful discussions with Jean Bidlot (ECMWF) are highly appreciated, and so are the anonymous reviewers for their thorough work. The work by the first author has been supported by the Research Council of Norway through the Centres of Excellence funding scheme, project number 223254 AMOS.

References

Akaike, H., 1980. Likelihood and Bayes Procedure, in: Bernado, J.M., Groot, M.H.D., Lindley, D.U., Smith, A.F.M. (Eds.), Bayesian Statistics. University Press, Valencia, pp. 143–166.

Antola, M., Solonen, A., Pyorre, J., 2017. Notorious Speed Through Water, in: Proc. of 2nd Hull Performance and Insight Conference, Ulrichshusen, Germany.

Beck, R., Cummins, W., Dalzell, J., Mandel, P., Webster, W., 1989. Vol. III: Motions in Waves and Controllability, in: Lewis, E. (Ed.), Principles of Naval Architecture, Second Revision. SNAME, pp. 1–188.

Bhattacharyya, R., 1978. Dynamics of Marine Vehicles. John Wiley & Sons.

Chen, X., Okada, T., Kawamura, Y., Mitsuyuki, T., 2019. Estimation of on-site directional wave spectra using measured hull stresses on a 14,000 TEU large container ships. Journal of Marine Science and Technology DOI: https://doi.org/10.1007/s00773-019-00673-w.

Copernicus Climate Change Service Information, 2020. ERA5: Fifth generation of ECMWF atmospheric reanalyses of the global climate. Copernicus Climate Change Service Climate Data Store (CDS), accessed 08-02-2020.

de Souza, F., 2019. Bayesian Estimation Of Directional Wave Spectrum Using Vessel Movements And Wave-Probes. Ph.D. thesis. Escola Politécnica Universidade de São Paulo, Brazil.

de Souza, F., Tannuri, E., de Mello, P., Franzini, G., Mas-Soler, J., Simos, A., 2018. Bayesian Estimation of Directional Wave-Spectrum Using Vessel Motions and Wave-Probes: Proposal and Preliminary Experimental Validation. J. Offshore Mechanics and Arctic Eng. 140, 041102:1–10.

ECMWF, 2017. Part VII: ECMWF Wave Model. Technical Report IFS Documentation Cy43r3. European Center For Medium-Range Weather Forecasts. Shinfield Park, Reading, RG2 9AX, England.

ECMWF, 2020. ERA5 hourly data on single levels from 1979 to present. `https://cds.climate.copernicus.eu/cdsapp#!/dataset/reanalysis-era5-single-levels?tab=overview`. Accessed: 30-01-2020.

Hasselaar, T., den Hollander, J., 2017. Uncertainty of Ship Speed Determination when Sailing in Waves, in: Proc. of 2nd Hull Performance and Insight Conference, Ulrichshusen, Germany.

Hersbach et al., 2020. The ERA5 Global Reanalysis. Quarterly Journal of the Royal Meteorological Society (*to be appear in*), DOI: 10.1002/qj.3803.

Hong, Y., Iseki, T., Nielsen, U., 2018. Short-term Variability of Cross-Spectral Analysis for Ship Responses in Waves, in: Proc. 17th Asia Navigation Conference, Chiba-city, Japan.

Hong, Y., Iseki, T., Nielsen, U., 2019. The Effect of Short-term Variability of Cross-Spectral Analysis on Wave Buoy Analogy, in: Proc. 29th ISOPE, Honolulu, HI, USA.

Iseki, T., 2010. Real-time Analysis of Higher Order Ship Motion Spectrum, in: Proc. of OMAE 2010, ASME, Shanghai, China.

Iseki, T., 2012. Non-stationary Ship Motion Analysis Using Discrete Wavelet Transform, in: Proc. 8th Int'l Conference on the Stability of Ships and Ocean Vehicles (STAB), Glasgow, Scotland.

Iseki, T., Nielsen, U., 2015. Study on a Short-term Variability of Ship Responses in Waves. Journal of Japan Institute of Navigation 132, 51–57.

Iseki, T., Ohtsu, K., 2000. Bayesian estimation of directional wave spectra based on ship motions. Control Engineering Practice 8, 215–219.

Iseki, T., Terada, D., 2003. Study on Real-time Estimation of the Ship Motion Cross Spectra. Journal of Marine Science and Technology 7, 157–163.

Komen, G., Cavaler, L., Donelan, M., Hasselmann, K., Hasselmann, S., Janssen, P., 1994. Dynamics and Modelling of Ocean Waves. Cambridge University Press.

Lindgren, G., Rychlik, I., Prevosto, M., 1999. Stochastic Doppler shift and encountered wave period distributions in Gaussian waves. Ocean Engineering 26, 507–518.

Mas-Soler, J., Simos, A., 2019. A Bayesian wave inference method accounting for nonlinearity related inaccuracies in motion RAOs. Applied Ocean Research (under review) .

Montazeri, N., Jensen, J., Nielsen, U., 2015. Uncertainties in ship-based estimation of waves and responses, in: Proc. of MTS/IEEE OCEANS15, Washington, DC, USA.

Montazeri, N., Nielsen, U., Jensen, J., 2016. Estimation of wind sea and swell using shipboard measurements - A refined parametric modelling approach. Applied Ocean Research 54, 73–86.

Nielsen, U., 2006. Estimations of on-site directional wave spectra from measured ship responses. Marine Structures 19, 33–69.

Nielsen, U., 2007. Response-based estimation of sea state parameters - influence of filtering. Ocean Engineering 34, 1797–1810.

Nielsen, U., 2008a. Introducing two hyperparameters in Bayesian estimation of wave spectra. Probabilistic Engineering Mechanics 23, 84–94.

Nielsen, U., 2008b. The wave buoy analogy - estimating high-frequency wave excitations. Applied Ocean Research 30, 100–106.

Nielsen, U., 2017. Transformation of a wave energy spectrum from encounter to absolute domain when observing from an advancing ship. Applied Ocean Research 69, 160–172.

Nielsen, U., 2018. Deriving the absolute wave spectrum from an encountered distribution of wave energy spectral densities. Ocean Engineering 165, 194–208.

Nielsen, U., Brodtkorb, A., 2018. Ship motion-based wave estimation using a spectral residual-calculation, in: Proc. of MTS/IEEE OCEANS18, Kobe, Japan.

Nielsen, U., Brodtkorb, A., Sørensen, A., 2018. A brute-force spectral approach for wave estimation using measured vessel motions. Marine Structures 60, 101–121.

Nielsen, U., Brodtkorb, A., Sørensen, A., 2019a. Sea state estimation using multiple ships simultaneously as sailing wave buoys. Applied Ocean Research 83, 65–76.

Nielsen, U., Dietz, J., 2020. Ocean wave spectrum estimation using measured vessel motions from an in-service container ship. Marine Structures 69, 102682.

Nielsen, U., Holt, P., 2020. Spatio-temporal variation in sea state parameters along ship route paths. J. Operational Oceanography (submitted for possible publication) .

Nielsen, U., Iseki, T., 2010. Estimation of sea state parameters from measured ship responses The Bayesian approach with fixed hyperparameters, in: Proc. of 29th OMAE, ASME, Shanghai, China.

Nielsen, U., Jensen, J., Pedersen, P., Ito, Y., 2011. Onboard monitoring of fatigue damage rates in the hull girder. Marine Structures 24, 182–206.

Nielsen, U., Johannesen, J., Bingham, H., Blanke, M., Joncquez, S., 2019b. Indirect Measurements of Added-wave Resistance On an In-service Container Ship, in: Proc. of 14th PRADS, Yokohama, Japan.

Nielsen, U., Lajic, Z., Jensen, J., 2012. Towards fault-tolerant decision support systems for ship operator guidance. Reliability Engineering and System Safety 104, 1–14.

Nieto-Borge, J., Reichert, K., Dittmer, J., 1999. Use of nautical radar as a wave monitoring instrument. Coastal Engineering 37, 331–342.

Oikonomakis, A., Galeazzi, R., Dietz, J., Nielsen, U., Holst, K., 2019. Application of Sensor Fusion to Drive Vessel Performance, in: Proc. of 4th Hull Performance and Insight Conference, Gubbio, Italy.

Pascoal, R., Guedes Soares, C., Sørensen, A.J., 2007. Ocean Wave Spectral Estimation Using Vessel Wave Frequency Motions. Journal of Offshore Mechanics and Arctic Engineering 129, 90–96.

Salvesen, N., Tuck, E.O., Faltinsen, O., 1970. Ship Motions and Sea Loads. Trans. SNAME 78, 250–287.

Sparano, J.V., Tannuri, E.A., Simos, A.N., Matos, V.L.F., 2008. On the Estimation of Directional Wave Spectrum Based on Stationary vessels 1st Order Motions: A New Set of Experimental Results, in: Proc. of OMAE'08, Lisbon, Portugal.

Stredulinsky, D.C., 2010. Quest Q319 Sea Trial Summary and Wave Fusion Analysis. Technical Report TM 2010-051. Defence Research and Development (DRDC) Canada - Atlantic. Dartmouth, NS, Canada.

Takami, T., Nielsen, U., Jensen, J., 2020. Estimation of Autocorrelation Function and Spectrum Density of Wave-induced Responses Using Prolate Spheroidal Wave Functions. Journal of Marine Science and Technology (submitted for possible publication) .

Tannuri, E.A., Sparano, J.V., Simos, A.N., Cruz, J.J.D., 2003. Estimating directional wave spectrum based on stationary ship motion measurements. Applied Ocean Research 25, 243–261.

Taudien, J., Bilén, S., 2018. Quantifying Long-Term Accuracy of Sonar Doppler Velocity Logs. IEEE Journal of Oceanic Engineering 43, 764–776.